Workshop on Visualisation in Environmental Sciences (EnvirVis) (2020)
S. Dutta and K. Feige and K. Rink and D. Zeckzer (Editors)

Visual Analysis of a Full-Scale-Emplacement Experiment in the Underground Rock Laboratory Mont Terri using Fiber Surfaces

F. Raith[1], C. Blecha[1], K. Rink[2], W. Wang[2], O. Kolditz[2,3], H. Shao[4], and G. Scheuermann[1]

[1]Institute of Computer Science, Leipzig University, Germany
[2]Department of Environmental Informatics, Helmholtz Center for Environmental Research, Leipzig, Germany
[3]Chair of Applied Environmental System Analysis, TU Dresden, Germany
[4]Federal Institute for Geosciences and Natural Resources, Hannover, Germany

Abstract

In the Underground Rock Laboratory Mont Terri, research has been conducted for over 20 years into the storage of radioactive waste in Opalinus Clay. The fitness for such storage depends on the prevailing geological material. Experiments and multiphysics simulations investigate the long-term changes in the Opalinus Clay. The resulting data are highly multivariate, and environmental scientists visually analyze the data using predefined color lookup tables. The fiber surfaces of Raith et al. offer the researchers a new approach for visual analysis. However, the existing algorithm for the calculation is subject to certain limitations due to special cases that lead to no or incomplete fiber surfaces. In this paper, we improve the fiber surface algorithm of Raith et al., which reduces numerical errors and accelerates the existing algorithm. This improvement also makes it possible that the interactor no longer needs to be closed and convex. We then use the Full-Scale Emplacement Experiment to show how the improved algorithm can help in the visual analysis of multivariate data.

CCS Concepts

• ***Human-centered computing*** → *Visual analytics; Scientific visualization;*

1. Introduction

The analysis of subsurface processes relies on a detailed knowledge of the precise location of geological horizons and fractures in the area of interest. Each geological formation has its own set of parameters, such as permeability and porosity of the material, thermal conductivity, specific heat capacity, and thermal expansivity. Given these parameters as well as a finite element mesh reproducing the structure of the subsurface volume enables researchers to numerically simulate specific phenomena such as groundwater flow, reactive transport, or the mechanic robustness of a specified medium under increasing stress. For a model simulating coupled thermo-hydro-mechanical processes, it is usual to calculate 20 or more parameters, including changes in temperature, pressure, saturation, displacement, stress, or strain.

Researchers in environmental sciences are used to visualizing data via plots of time series or displaying scalar data on a plane given predefined color lookup tables. However, complex models simulate a large number of variables, many of which are dependent on one another. Therefore, it is necessary to enable a meaningful visual exploration of complex multivariate data using data subsets generated based on non-trivial criteria, such as level sets in multivariate space.

One technique that is suitable for this purpose is fiber surfaces, as they offer the possibility to work with multivariate level sets. However, the existing methods from the work of Raith et al. [RBN*19] have to be extended to overcome fundamental limitations. The extensions of the method reduce numerical errors, allow the investigation of exactly planar tetrahedra, and offer the possibility to use the fiber surface itself as an interactor. This superiority of the improved algorithm is demonstrated by a typical exemplary data set of multiphysics simulation.

2. Related Work

The role of visual analysis of multivariate data has been increasing for decades. A survey on visualizing multivariate scientific data by Fuchs and Hauser [FH09] introduces suitable visualization techniques and identifies the most promising approaches. The visual analysis of multivariate data was also mentioned as one of the challenges in the Dagstuhl Seminar 2014 [HCJ*14]. Glyphs were mentioned as a standard technique for the analysis of multivariate data in Chung et al. [CLKH14], and the importance of feature-based techniques was emphasized in the work of Obermaier et al. [OP14] and Carr [Car14].

Direct multiphysics analyzes are rare. One example has been

DOI: 10.2312/envirvis.20201093

published by Perdikaris et al. [PIG*16] and analyzes flow-structure interactions in a high-resolution numerical simulation of blood flow within a brain aneurysm as well as the structural integrity of the arterial wall.

Most multivariate techniques for visual analysis are based on univariate data. The exploration of multi- or at least bivariate data sets is, therefore, a challenging research topic. Carr et al. [CGT*15] made an important contribution by introducing an approach to the extraction of fiber surfaces, i.e. the two-dimensional equivalent of isosurfaces for a bivariate field. Specifically, fiber surfaces are the inverse image of a polygon (or polyline) in the bivariate field. Klacansky et al. [KTCG16] improved the above approach by proposing a fast and accurate extraction method.

Jankowai and Hotz [JH18] present a general approach for the visualization of multivariate data. They use feature level-sets and traits. They define standard isosurfaces and the fiber surfaces of Carr et al. [CGT*15] as special cases of those. The user can select single values as well as features. From this, a distance field between the features in the attribute space is calculated and projected into the spatial domain, where it is visualized by volume rendering or marching cubes.

Sauber et al. [STS06] use a different approach, showing correlations between three-dimensional scalar fields by introducing a multi-field graph. Each node corresponds to a correlation field that combines at least two fields. This approach allows deciding which correlation fields should be investigated. This work has been improved by Nagaraj et al. [NNN11] by introducing another measure of comparison.

The first approaches of automatic identification of important regions have been shown in the early work of Jänicke et al. [JWSK07]. They employ local statistical complexities described by partial differential equations. This approach differs from our interactive selection approach.

In this work, the fiber surfaces of Raith et al. [RBN*19] are used. Here, the fiber surfaces of Carr et al. [CGT*15] are extended to a three-dimensional attribute space for the analysis of symmetric, three-dimensional second-order tensor fields. These surfaces are defined as fiber surfaces of invariant space, i.e., as models of surfaces in the range of a complete set of invariants. Based on this, Blecha et al. [BRS*19] used fiber surfaces to study a multiphysics simulation of a generic model of a nuclear waste repository.

Blecha et al. [BRP*20] generalized the fiber surfaces of Raith et al. [RBN*19] to work with any number of scalar fields defined on a tetrahedral mesh, i.e., from $\mathbb{R}^3$ to $\mathbb{R}^n$ in the range. They introduced a new fiber surface extraction algorithm which does not only extracts the triangles of the fiber surface components but also refines the tetrahedral input grid to the subset, which lies inside the restraining hypersurfaces. The n-dimensional hypersurface is built using multiple convex objects in multiple three-dimensional views of subspaces of the whole attribute space. Advancing that approach, the algorithm used in this work can work with interactors that do not have to be closed and convex.

In the following, we will apply an improved fiber surface algorithm to simulation results based on an experiment conducted in the Underground Rock Laboratory Mont Terri, reducing numerical errors, and simultaneously accelerating the algorithm.

3. Underground Rock Laboratory Mont Terri

The Underground Rock Laboratory (URL) Mont Terri [BM17] was established in the Canton of Jura in northwestern Switzerland in 1996. It is located more than 250 m under the Jurassic Mountains in a thick layer of Opalinus Clay. When considering the deep geological storage of radioactive waste, this type of claystone is of particular interest to researchers, because Opalinus Clay is almost completely water-impermeable and therefore considered an alternative to the disposal in crystalline or salt rock. The laboratory is used for research purposes only, and no radioactive waste is actually stored there, nor will the tunnel system be used for this purpose at any point in the future. Instead, more than 140 experiments have so far been conducted regarding the development of methodologies and the characterization of Opalinus Clay. These experiments have advanced the determination of rock parameters using innovative borehole geophysics, improved the methodology for characterization of pore-water and microbial activity, and gained a new understanding of diffusion and retention processes of radionuclides in and through claystones. Demonstration experiments allow tests on a 1:1 scale to be carried out over a long period, ranging from years to decades. Numerical simulations support many experiments for planning purposes and process understanding (see Figure 1). The numerical results of one of these experiments, the Full-Scale Emplacement (FE) experiment, will be used to demonstrate the potential of our improved fiber surface algorithm.

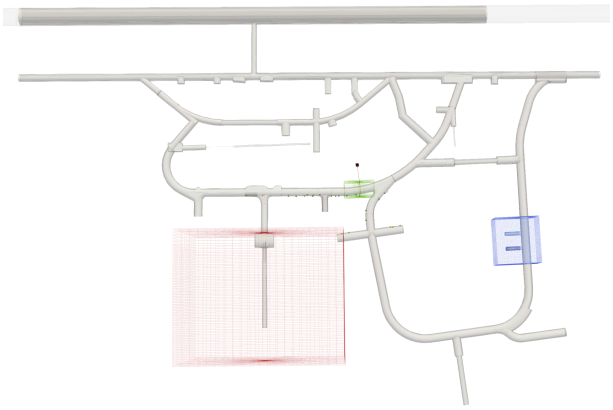

Figure 1: *Overview of the Underground Rock Laboratory Mont Terri. Domains of models supplementing current experiments are outlined as wireframe meshes, incl. the Full-Scale Emplacement experiment shown in red (data source for tunnel system: swisstopo)*

The FE Experiment aims to model the construction, waste emplacement, backfilling, and early stage evolution of spent fuel or high-level waste repository tunnel. Instead of canisters containing radioactive material, heaters are placed on pedestals within a tunnel of 10 m length, and 2.3 m diameter. Scoping calculations indicate that the surface of the heaters will reach a peak temperature of 100 to 195 degrees Celsius, depending on the buffer material used. The end of the tunnel is filled with concrete and bentonite,

the remaining open space in the tunnel is filled with a selection of special backfilling materials (incl. the heater elements themselves) and then sealed by a concrete plug with a thickness of 1.4 m (see Figure 2). More than 1,600 sensors in the near- and far-field are observing the effects of the experiment on the surrounding formation of Opalinus Clay, measuring temperature, relative humidity, deformation, pore water pressure, total pressure, and many other parameters [MGV*17].

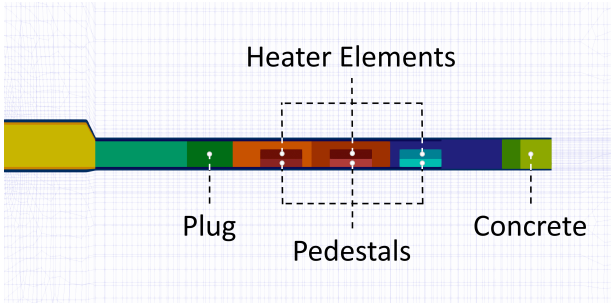

Figure 2: *Set-up of the Full-Scale-Emplacement experiment within the finite element mesh of the model domain.*

Numerical simulation codes are used to simulate the Thermo-Hydro-Mechanical (THM) processes in and near the tunnel as well as the far-field, to assess the uncertainty of the propagation of parameters. Based on the specification by the FE-Modelling Task Force [AM19], a numerical model of the FE experiment has been set up in OpenGeoSys [KBB*12, KSG*18, BFK*19]. Required sub-tasks include the verification of both code and calculation using generic benchmarks, the back-analyses of THM-observations using monitoring data for model calibration, and the validation of the model itself by predicting the evolution of parameters given changing thermal loads. The model domain has a size of $100 \times 100 \times 80\,m$ with the tunnel located in the center of the block. The domain of the OpenGeoSys-model consists of 170,000 hexahedra. The tunnel itself (incl. heaters, pedestals, backfill, shotcrete, and disturbance zone) and the near field use a very fine discretization, with elements becoming larger with increasing distance to the tunnel. Input data and simulation results have been pre- and post-processed, respectively, using the OpenGeoSys Data Explorer [RBK14] and ParaView [AGL05]. The simulations calculate the development of temperature, pressure, saturation, velocity, stress, strain, and displacement over 5,800 days. The output data used for the subsequent visualization via our fiber surface algorithm included 115 timesteps at increasing intervals, resulting in a total of about 16 GB of data.

4. Improved Fiber Surface Extraction

In the work of Raith et al. [RBN*19], special cases were considered where the calculation of the fiber surfaces leads to no or incomplete fiber surfaces. One of these cases is the numerical error in the calculation of the intersection points. These errors occur in small tetrahedra, especially in the repeated calculation of intersection points. Another case is perfectly planar tetrahedra. This case was not considered in the algorithm of Raith et al. because there was no bijection between the invariant space and the physical domain. As a result, these cases led to holes in the fiber surfaces.

In the data sets considered here, too many of these errors occurred, so that a visual analysis was no longer possible (see Figure 3a). To solve this problem, we redesigned the extraction algorithm to reduce the numerical errors so that that becomes possible to process planar tetrahedra.

In a preprocessing step, the modified algorithm first calculates the Hesse normal form of all interactor triangles to reduce the numerical errors in a double calculation. In a second preprocessing step, we test if the points of a tetrahedral cell are on different sides of a plane of the triangles. If not, no interaction is possible. Otherwise, we use a new algorithm to calculate the intersection points between the co-domain tetrahedra and the triangle of the interactor. The new calculation of the intersection points is based on a classical clipping algorithm from computer graphics, the Sutherland-Hodgman algorithm [SH74].

Algorithm 1 Calculation of a Fiber Surface with clipping algorithm

Require: Grid *OSG* in Object Space, Intersecting Tetrahedra *Tet*, list of triangles *Tri* from interactor
preprocessing Save Hesse normal form for all $tri \in Tri$ in *Normals*
for all tetrahedra $tet \in Tet$ **do**
  for all triangles $tri \in Tri$ **do** ▷ subject polygons
    if Test intersection tet and tri **then** ▷ used *Normals*
      set $PointList = p \in tri$
      for all face $f \in tet$ **do** ▷ clip polygons
        for all points $p_i, p_j \in PointList$ **do**
          calculate distances of p_i and p_j to face f
          if both distances are smaller or equal to 0 **then**
            add both points to *NewPointList*
            projection both points in *OSG*
          else if only one distance is smaller or equal to 0 **then**
            add inner point to *NewPointList*
            projection inner point in *OSG*
            add *intersectionpoint* between $\overline{p_i p_j}$ and face f to *NewPointList*
            projection *intersectionpoint* in *OSG*
          else if both distances are greater 0 **then**
            do nothing
          end if
        end for
        set $PointList = NewPointList$
      end for
    end if
    triangulation of the *intersectionPlane*
  end for
end for

This algorithm (see Algorithm 1) requires a list of all points in the subject polygon and the clip polygon as input to calculate the intersection points. All the interactor triangles are used as subject polygons, and the faces of the co-domain tetrahedra are used as clip polygons. So each triangle in the interactor is clipped with the faces of the tetrahedra. The resulting intersections from the co-domain are simultaneously projected to the domain.

A further advantage of using the clipping algorithm is that the sequence of the intersection points is known, which simplifies the triangulation of the resulting cut surface. These adjustments simplify and accelerate the algorithm and make it possible to investigate areas that could not be detected before (see Figure 3b).

A side-effect of the new algorithm is that the previous assumption from Raith et al., stating that the interactor must be closed and convex, is now obsolete.

(a) *Fiber surface without clipping algorithm.*

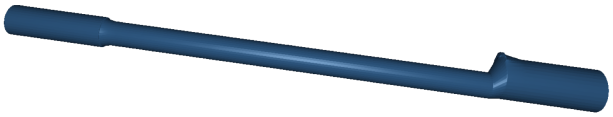

(b) *Fiber surface with clipping Algorithm.*

Figure 3: *Extraction of the fiber surface from an attribute space (Temperature-Saturation-Stress$_{zz}$) for a specific area around the tunnel. Figure 3a shows the extraction with the Fibersurface algorithm by Raith et al. and Figure 3b shows the improved Fibersurface algorithm from this work.*

5. Visual Analysis

In the past, visual analysis of THM-simulation results of the FE experiment via OpenGeoSys was done via Paraview [AGL05]. Several simulated variables of interest are displayed in parallel, and a suitable color lookup table is chosen. Developments over time, such as the propagation of temperature during the heating phase of the experiment, the resulting desaturation of the claystone and the subsequent changes in the vertical stress in the formation around the tunnel, are explored during the analysis of the model results (see Figure 4). Results of that analysis obviously depend on the intuition and experience of the scientist performing said analysis, as effects may only become apparent by correct placement of the clipping plane and the selection (and possibly the adjustment) of suitable color lookup tables (LUTs). Even then, only parts of the data can be viewed at a time, and it is difficult to understand the propagation of variables within 3D space thoroughly.

The improved fiber surface algorithm allows the user to visualize the data in several ways. Some particularly suitable approaches for the analysis of results from the FE experiment are briefly introduced in the following.

Extract Fiber Surface

The improved fiber surface algorithm allows the user to view the entire object space at once and select a linear combination of three attributes from the simulation results. This is the simplest analysis

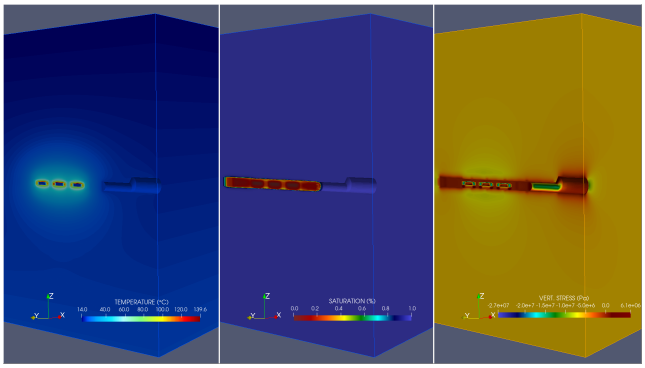

Figure 4: *Visual exploration of three variables (temperature, saturation, vertical stress) via ParaView.*

option, and it is very effective when a region of interest needs to be analyzed in more detail. Figure 5a uses an attribute space consisting of eigenvalues of the stress field. The λ_{major} is mapped to the x-axis, the $\lambda_{intermediate}$ to the y-axis and the λ_{minor} to the z-axis. The blue wireframe is the mapping of the object to the attribute space, and the red wireframe is a cube interactor used to select a conspicuous area. The intersection between the interactor and the wireframe forms the fiber surface. This fiber surface is shown in object space in Figure 5b. Besides, the temperature is displayed on this surface to visualize the relationship.

The three heaters and the surrounding tunnel are clearly visible in object space. At the timestep shown, the temperature on the surface of the heaters is increasing strongly, but due to the backfill material, the surrounding tunnel is getting only marginally warmer. With the fiber surface in Figure 5b, it becomes immediately obvious that the stresses are asymmetrically propagated during the FE experiment. This effect would have been complicated to detect using the visualization techniques used before (i.e. a combination of LUTs and clipping).

Sliding Fiber Surface

Another potential visual analysis creates a fiber surface with a slider through attribute space. With this technique, it becomes easy to give a first impression of the entire attribute space to quickly analyze simulation errors or the general distribution in the attribute space. It is also possible to analyze an area of interest where it is not possible to identify a single position.

In Figure 6 uses the same attribute space from the simulation results of the FE experiment that has been used as in Figure 4. Here, the temperature is mapped to the x-axis, saturation to the y-axis, and vertical stress to the z-axis. The attribute space can be recognized by the interactor in the Figures 6a, 6c, 6e. Figures 6b, 6d, 6f show the corresponding fiber surface in object space. In this example, we investigated a region where the saturation is very high but has not yet reached the maximum. The interactor is sliding along the z-axis through the attribute space. Temperature is again mapped onto the fiber surface, showing the areas around the heater elements illustrated in Figure 2. This area is especially interesting for the

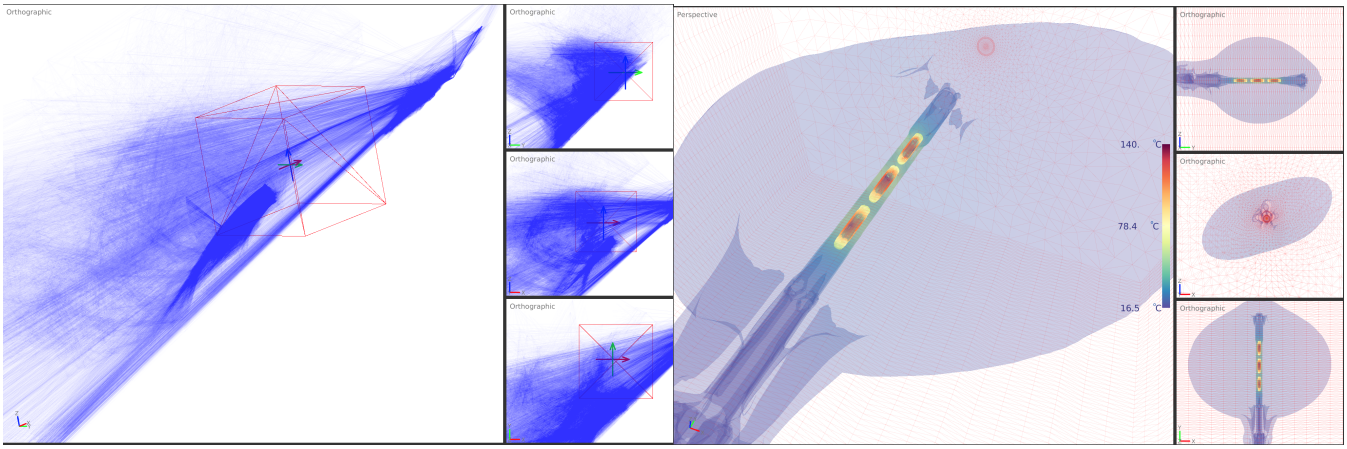

(a) *Attribute space* **(b)** *Object space*

Figure 5: *Interaction of the interactor (red) with the attribute space of the FE experiment (blue) (5a) and visualization of the extracted fiber surfaces in the object space (5b). The temperature is mapped to this fiber surface.*

engineers because the effects of increased temperature on the surrounding tunnel and clay formation are key questions of the experiment.

Connected Fiber Surface

Our final visual analysis uses connected fiber surfaces. These become possible because interactors no longer have to be closed and convex. The calculated fiber surface itself is used as a new interactor in another attribute space to display the values in that second space. This method is especially interesting when an interactor from the object space is displayed in the attribute space and is directly mapped back into the object space as a new interactor. Because the tetrahedra penetrate each other in attribute space, not only the interactor in object space is identified again but also all areas that have the same combination of attributes as the original interactor.

In Figure 7, this method is applied to the simulation results of the FE experiment. First, a simple interactor is used to extract a fiber surface from the attribute space in Figure 4, which represents the three chambers and the tunnel entrance (see Figure 7a). From this, the marked blue chamber is selected and used as the new interactor (see Figure 7b). The blue interactor is now mapped into the attribute space of the stress eigenvalues and used as the new interactor (see Figure 7c). The resulting fiber surface created in object space is shown in Figure 7d, covering not only the original interactor but also all other areas with the same attribute combination. The temperature has been mapped onto the fiber surface again, to improve analysis.

6. Conclusion

In this work, we used the data from the underground rock laboratory Mont Terri, where a large number of experiments on the storage of radioactive waste in claystone are conducted. For the results of a multiphysics simulation of one of these experiments, the full-scale emplacement experiment, we presented an improved fiber surface extraction algorithm for visual analysis. This improvement allows us to study perfectly planar tetrahedra and reduces the numerical errors of the original algorithm. Besides, the algorithm was redesigned to enable the visual analysis of these perfectly planar tetrahedra, and a clipping algorithm was used to calculate the intersections between the interactor triangles and the object tetrahedra. The improved fiber surface algorithm facilities several novel ways to visualize data, some of which have been applied to numerical results of the FE experiment. We have shown that with the fiber surface algorithm, the user can get an overview of the whole object domain reasonably fast. Previously hard to detect phenomena, such as the asymmetry of the stress propagation, become reasonably easy to detect. A particularly exciting prospect for visual analysis is the use of the fiber surface itself as an interactor. This method has become possible because the interactor does not have to be closed and convex.

With this new algorithm, their much potential for future analyses. Here, only a first overview of the FE experiment could be given. These investigations need to be extended and refined in collaboration with domain scientists and may also be applied to other experiments from the URL Mont Terri. The work of Blecha et al. [BRP*20], which extends the fiber surface to n-dimensions, could also contribute to a more thorough investigation. Furthermore, interactivity suffers from the use of complex interactors, which is why a corresponding acceleration of the algorithm is an important goal for future work. Moreover, automatic recognition of interesting areas in the attribute space is also an extension that would substantially support researchers during the analysis of multivariate data.

Acknowledgements: We deeply acknowledge the funding of the iCROSS-Project (Integrity of nuclear waste repository systems – Cross-scale system understanding and analysis) by the Federal

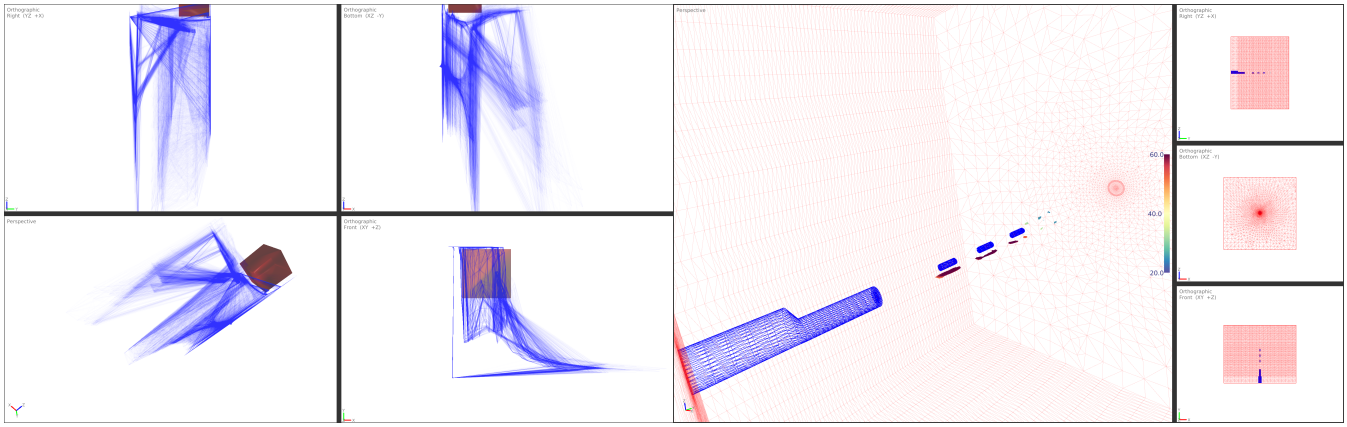

(a) *Attribute space* **(b)** *Object space*

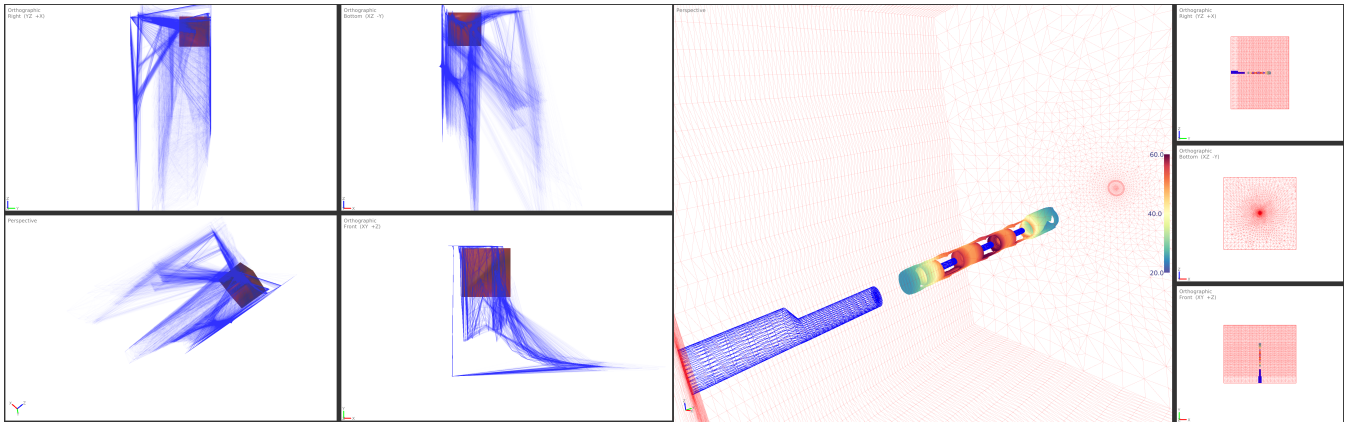

(c) *Attribute space* **(d)** *Object space*

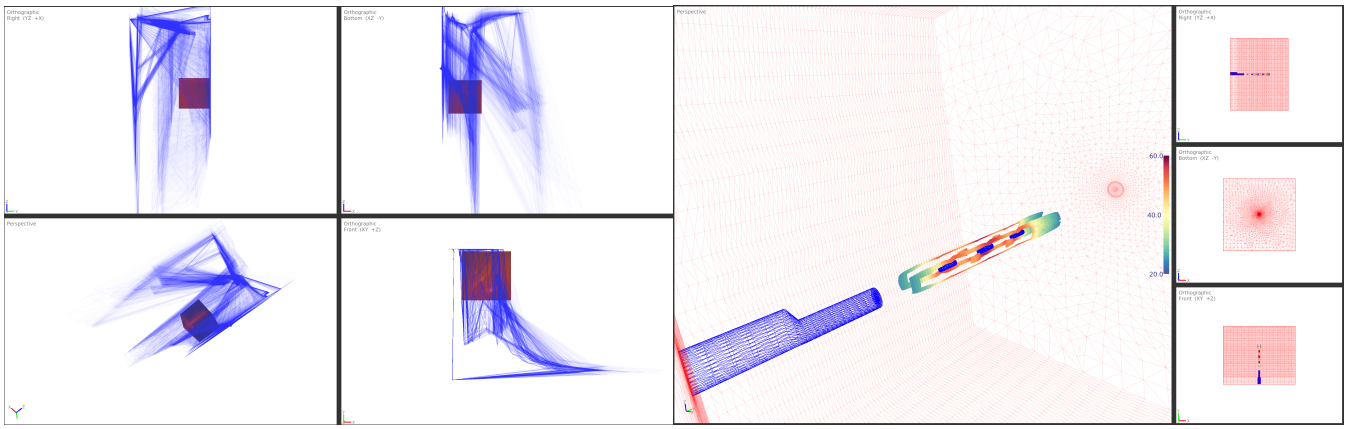

(e) *Attribute space* **(f)** *Object space*

Figure 6: *Selection of 3 slider positions. The attribute space shows the eigen stress (6a, 6c, 6e) and in the interactor (red). In the object space (6b, 6d, 6f), the temperature is mapped to the fiber surface. For better localization, the tunnel entrance and the 3 inclusions are shown as blue wireframe.*

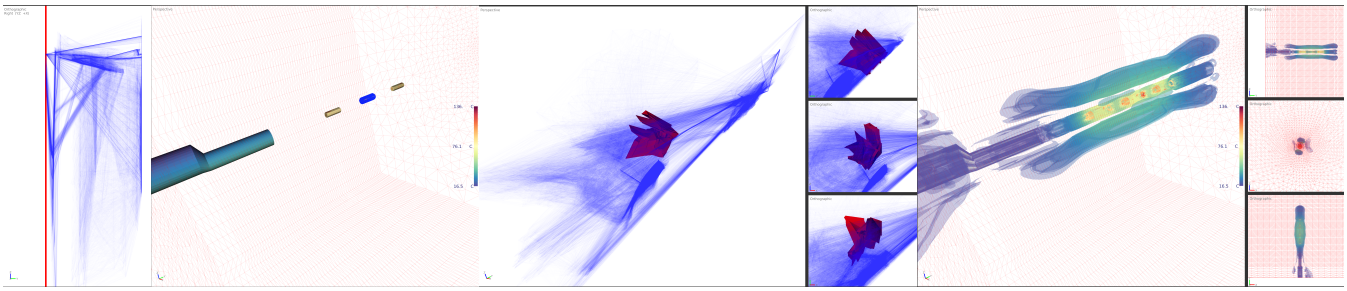

(a) *Attribute space* **(b)** *Object space* **(c)** *Attribute space* **(d)** *Object space*

Figure 7: *Extraction of a fiber surface from the attribute space (Temperature-Saturation-Stress$_{zz}$) with a simple interactor (7a). A section (blue) of the fiber surface is marked and used as a new interactor (7b). With this interactor a fiber surface in the attribute space (λ_{major}-$\lambda_{intermediate}$-λ_{minor}) is extracted (7c), which is mapped back into the object space (7d). The temperature was mapped to this fiber surface.*

Ministry of Research and Education (grant number 02NUK053E, gefördert vom BMBF) and Helmholtz Association through the Impulse and Networking Funds (grant number SO-093). We are grateful to the Mont Terri consortium for supporting the VR Task which is also partly funded by the iCROSS project. In addition, we would like to thank swisstopo, the National Cooperative for the Disposal of Radioactive Waste (NAGRA), the Gesellschaft für Anlagen- und Reaktorsicherheit (GRS), Andra, RWMO, and Andrés Alcolea Rodriguez (HydroGeoModels AG) for providing data and support.

References

[AGL05] AHRENS J., GEVECI B., LAW C.: ParaView: An End-User Tool for Large Data Visualization. In *The Visualization Handbook*, Hansen C., Johnson C., (Eds.). Elsevier, 2005. 3, 4

[AM19] ALCOLEA A., MARSCHALL P.: *FE-Modelling Task Force / Task 1: Validation of thermally induced THM effects in the rock around the FE-tunnel – Specification of Subtask 1.1*. Tech. rep., Mont Terri Project, 2019. 3

[BFK*19] BILKE L., FLEMISCH B., KALBACHER T., ET AL.: Development of open-source porous media simulators: principles and experiences. *Transport Porous Media 130*, 1 (2019), 337–361. doi:10.1007/s11242-019-01310-1. 3

[BM17] BOSSARD P., MILNESS A. G. (Eds.): *Mont Terri Rock Laboratory, 20 Years – Two Decades of Research and Experimentation on Claystones for Geological Disposal of Radioactive Waste*. Springer Cham, 2017. ISBN:978-3-319-70457-9. 2

[BRP*20] BLECHA C., RAITH F., PRÄGER A. J., NAGEL T., KOLDITZ O., MASSMANN J., RÖBER N., BÖTTINGER M., SCHEUERMANN G.: Fiber Surfaces for many Variables. In *Conditionally accepted EuroVis 2020* (2020). 2, 5

[BRS*19] BLECHA C., RAITH F., SCHEUERMANN G., NAGEL T., KOLDITZ O., MASSMANN J.: Analysis Of Coupled Thermo-Hydro-Mechanical Simulations Of A Generic Nuclear Waste Repository In Clay Rock Using Fiber Surfaces. In *2019 IEEE Pacific Visualization Symposium (PacificVis)* (April 2019), pp. 189–201. doi:10.1109/PacificVis.2019.00030. 2

[Car14] CARR H.: Feature Analysis in Multifields. In *Scientific Visualization: Uncertainty, Multifield, Biomedical, and Scalable Visualization*, Mathematics and Visualization. Springer, 2014, pp. 197–204. 1

[CGT*15] CARR H., GENG Z., TIERNY J., CHATTOPADHYAY A., KNOLL A.: Fiber Surfaces: Generalizing Isosurfaces To Bivariate Data. In *Computer Graphics Forum* (2015), vol. 34, Wiley Online Library, pp. 241–250. 2

[CLKH14] CHUNG D. H., LARAMEE R. S., KEHRER J., HAUSER H.: Glyph-Based Multi-field Visualization. In *Scientific Visualization*. Springer, 2014, pp. 129–137. 1

[FH09] FUCHS R., HAUSER H.: Visualization of multi-variate scientific data. *Computer Graphics Forum 28*, 6 (2009), 1670–1690. URL: https://www.cg.tuwien.ac.at/research/publications/2009/fuchs-vom-2009/. 1

[HCJ*14] HANSEN C., CHEN M., JOHNSON C., KAUFMAN A., HAGEN H.: *Scientific Visualization: Uncertainty, Multifield, Biomedical, and Scalable Visualization*. Mathematics and Visualization. Springer, 01 2014. 1

[JH18] JANKOWAI J., HOTZ I.: Feature Level-Sets: Generalizing Iso-Surfaces To Multi-Variate Data. *IEEE transactions on visualization and computer graphics* (2018), 1–1. 2

[JWSK07] JANICKE H., WIEBEL A., SCHEUERMANN G., KOLLMANN W.: Multifield visualization using local statistical complexity. *IEEE Transactions on Visualization and Computer Graphics 13*, 6 (2007), 1384–1391. 2

[KBB*12] KOLDITZ O., BAUER S., BILKE L., ET AL.: OpenGeoSys: An open source initiative for numerical simulation of thermo-hydro-mechanical/ chemical (THM/C) processes in porous media. *Environ Earth Sci 67*, 2 (2012), 589–599. doi:10.1007/s12665-012-1546-x. 3

[KSG*18] KOLDITZ O., SHAO H., GÖRKE U.-J., WANG W., BAUER S. (Eds.): *Thermo-Hydro-Mechanical-Chemical Processes in Fractured Porous Media: Modelling and Benchmarking*. Springer Berlin-Heidelberg, 2018. ISBN:978-3-319-68224-2. 3

[KTCG16] KLACANSKY P., TIERNY J., CARR H., GENG Z.: Fast And Exact Fiber Surfaces For Tetrahedral Meshes. *IEEE transactions on visualization and computer graphics 23*, 7 (2016), 1782–1795. 2

[MGV*17] MÜLLER H., GARITTE B., VOGT T., ET AL.: Implementation of the full-scale emplacement (FE) experiment at the Mont Terri rock laboratory. *Swiss J Geosci 110* (2017), 287–306. doi:10.1007/s00015-016-0251-2. 3

[NNN11] NAGARAJ S., NATARAJAN V., NANJUNDIAH R. S.: A gradient-based comparison measure for visual analysis of multifield data. *Computer Graphics Forum 30*, 3 (2011), 1101–1110. URL: https://onlinelibrary.wiley.com/doi/abs/10.1111/j.1467-8659.2011.01959.x, arXiv:https://onlinelibrary.wiley.com/doi/pdf/10.1111/j.1467-8659.2011.01959.x, doi:10.1111/j.1467-8659.2011.01959.x. 2

[OP14] OBERMAIER H., PEIKERT R.: Feature-Based Visualization of Multifields. In *Scientific Visualization: Uncertainty, Multifield, Biomedical, and Scalable Visualization*, Mathematics and Visualization. Springer, 2014, pp. 189–196. 1

[PIG*16] PERDIKARIS P., INSLEY J. A., GRINBERG L., YU Y., PAPKA M. E., KARNIADAKIS G. E.: Visualizing multiphysics, fluid-structure interaction phenomena in intracranial aneurysms. *Parallel Computing 55* (2016), 9 – 16. Visualization and Data Analytics for Scientific Discovery. URL: http://www.sciencedirect.com/science/article/pii/S016781911500160X, doi:https://doi.org/10.1016/j.parco.2015.10.016. 2

[RBK14] RINK K., BILKE L., KOLDITZ O.: Visualisation Strategies for Environmental Modelling Data. *Env Earth Sci 72*, 10 (2014), 3857–3868. doi:10.1007/s12665-013-2970-2. 3

[RBN*19] RAITH F., BLECHA C., NAGEL T., PARISIO F., KOLDITZ O., GÜNTHER F., STOMMEL M., SCHEUERMANN G.: Tensor Field Visualization Using Fiber Surfaces Of Invariant Space. *IEEE transactions on visualization and computer graphics 25*, 1 (2019), 1122–1131. 1, 2, 3

[SH74] SUTHERLAND I. E., HODGMAN G. W.: Reentrant polygon clipping. *Communications of the ACM 17*, 1 (1974), 32–42. 3

[STS06] SAUBER N., THEISEL H., SEIDEL H.: Multifield-graphs: An approach to visualizing correlations in multifield scalar data. *IEEE Transactions on Visualization and Computer Graphics 12*, 5 (Sep. 2006), 917–924. doi:10.1109/TVCG.2006.165. 2